

LETTER TO THE EDITOR

A shocking outcome: Jet dynamics and polarimetric signatures of the multi-band flare in blazar OJ 248

G. F. Paraschos¹ 

¹Max-Planck-Institut für Radioastronomie, Auf dem Hügel 69, D-53121 Bonn, Germany
e-mail: gfparaschos@mpi-fr-bonn.mpg.de

Received -; accepted -

ABSTRACT

The connection between γ -ray flares and blazars is a topic of active research, with few sources exhibiting distinct enough such outbursts to be able to conclusively connect them to features in their jet morphology. Here we present an investigation of the sole γ -ray flare of the blazar OJ 248 thus far, in association with its jet structure, as revealed by very long baseline interferometry (VLBI). We find that throughout the course of the γ -ray flare, the fractional linear polarisation increases in the jet of OJ 248, and the VLBI electric vector position angles (EVPAs) turn perpendicular to the bulk jet flow. We interpret this behaviour as a moving shock, travelling through a recollimation shock and upscattering photons via the inverse Compton scattering process, producing a γ -ray flare; we discuss possible mechanisms. Our hypothesised shock-shock interaction scenario is a viable mechanism to induce such EVPA rotations in both optical and radio bands.

Key words. Galaxies: jets – Galaxies: active – Galaxies: individual: OJ 248 (0827+243) – Techniques: interferometric – Techniques: high angular resolution

1. Introduction

The flat spectrum radio quasar (FSRQ) OJ 248 (0827+243), located at $z = 0.939$ (Hewett & Wild 2010), is noted to be a bright, γ -ray loud blazar (Abdo et al. 2010). Its powerful radio jet, propelled by a central supermassive black hole ($M_{\text{dyn}} \sim 8 \times 10^8 M_{\odot}$; Zhang et al. 2024), has been resolved at multiple scales with very long baseline interferometry (VLBI). At parsec-scales the OJ 248 jet exhibits superluminal motion (Jorstad et al. 2001; Piner et al. 2006), while at larger scales (Price et al. 1993) its bent morphology coincides with X-ray emission detected with the *Chandra X-ray Observatory* (Jorstad & Marscher 2004, 2006).

Variability has also been observed in OJ 248, both in total intensity optical and near infrared light curves (in terms of flaring activity, e.g. Villata et al. 1997; Raiteri et al. 1998; Enya et al. 2002; Marchesini et al. 2016), as well as at VLBI scales (in terms of morphological changes, e.g. Marscher & Broderick 1983). Such VLBI-detected structural changes in the jet morphology are thought to be caused by the dominating magnetic fields, which directly influence the jet collimation and evolution. Most recently, a prominent multi-band flare was reported in Carnerero et al. (2015), which peaked in 2013, spanning from radio wavelengths to γ -rays, followed by a prolonged period of quiescence (McCall et al. 2024). The delay between optical bands and γ -rays was marginal, whereas a two month delay was found between γ -rays and the millimetre radio band. In parallel, the optical polarisation percentage rose sixfold during the multi-band flare onset (Carnerero et al. 2015). Here we explore the connection between this multi-band flare and structural changes in its parsec-scale jet, manifested in linear polarisation and electric vector position angle (EVPA) rotations, seeking a better understanding of the underlying driving mechanisms. In Sect. 2 we

briefly present the observations and expand on our results. Section 3 we discuss a possible of the flaring event and in Sect. 4 we summarise our findings.

2. Methods

2.1. Observations and data analysis

For this work we utilised publicly available VLBI data obtained with the Very Long Baseline Array (VLBA) at 43 GHz as part of the VLBA-BU-BLAZAR programme¹. A detailed description of the observations and how the data that we used were calibrated in total intensity and polarisation is reported in Jorstad et al. (2017). During the time frame we review here, corresponding to modified Julian dates (MJD) between 56152 and 56349, OJ 248 was observed eight times. For these epochs, we extracted total intensity, linear polarisation, and EVPA information using the geometrical model-fitting capability of the *eht-imaging* framework (Chael et al. 2016; Roelofs et al. 2023). In a nutshell, geometrical model-fitting describes the structural and morphological properties of the observed emission, typically using simple parametric components such as Gaussian functions. The advantage of this approach lies in the fact that the jet can be decomposed into such Gaussian components, for each of which all relevant measurables are identifiable. This makes it easier to track the connection between jet activity and light curve variability as manifested through multi-band flares. Details about our modelling approach can be found in Paraschos et al. (2024b) and Paraschos et al. (2024c). The accompanying weekly binned γ -ray light curve was obtained from the Fermi Large Area Telescope Collaboration (Fermi-LAT; see Atwood

¹ <https://www.bu.edu/blazars/BEAM-ME.html>

et al. 2009; Ajello et al. 2020) repository², containing publicly available daily, weekly, and monthly binned data.

2.2. Results

Our analysis revealed that the OJ248 jet is best approximated by two components in the time frame of interest, labelled as ‘C’ (core, which we assumed to be stationary) and ‘Q1’. In this framework C corresponds to the compact, optically thick region near the jet base and Q1 to the more extended jet emission. Figure 1 displays the progression in the evolution of the overall jet morphology, with the parameters of the two components being listed in Table 1. The parameters include the component identification, observation date, flux density (F0), full width at half maximum (FWHM) of each component, the position of Q1 relative to C, their fractional polarisation m , and their EVPAs. Our results show that the extended jet (Q1) started out in a quiescent state (with $m_C > m_{Q1}$), then m_{Q1} increased during the entirety of the γ -ray flare event duration (reaching a peak of $m_{Q1} \sim 15\%$), before returning to its quiescent state again in the last epoch. Simultaneously, $m_C \sim 10\%$ before and after the flare but decreased to approximately half during it. Interestingly, the EVPAs in C appear aligned to the bulk jet flow before and after the γ -ray flare event, while turning perpendicular to it during the event. Furthermore, the overall flux density seems to increase during the event but then remains on higher levels. Finally, the distance between Q1 and C is slowly increasing ($\mu = 0.17 \pm 0.06$ mas/yr, which is slower than the velocity of the source reported in the 1990s; see Jorstad et al. 2001).

Simultaneously, the γ -ray light-curve shown in the top panel of Fig. 2 exhibited a very bright flare, the prominence of which has not been repeated since then. In parallel, a multi-band flare was also reported in the optical, near IR, and millimetre radio bands by Carnerero et al. (2015). The authors also found an increase in the polarised flux and rotations in the optical EVPAs (although a clear trend was lacking). In the middle and bottom panels of Fig. 2 we over-plotted the radio wavelength EVPAs and flux density of C and Q1 during the flaring event. We can clearly observe that the γ -ray flare is accompanied by an EVPA rotation in the radio as well, accompanied by a flux increase.

3. Discussion

The true nature of γ -ray flares is one of the fundamental open questions related to jet activity. In order to produce such a flare, a region of internal photons must be present for synchrotron self-Compton (Königl 1981) scattering (inverse Compton-scattering) to occur; the so-called blazar zone (see, e.g. Hovatta & Lindfors 2019, for a review). The exact location of this flare origin region with regard to the radio core observed with VLBI, remains unclear. Both upstream (near the central engine) and downstream (extended jet) locations of the VLBI core have recently been reported as the possible origin of flares and this includes blazars (e.g. Rani et al. 2018) and, interestingly, radio galaxies as well (e.g. Paraschos et al. 2023), with the latter also showing evidence of a connection to jet feature ejections (Agudo 2013; Paraschos et al. 2022). Furthermore, jets could be transversely stratified, for example exhibiting a so-called ‘spine-sheath’ geometry, where a fast inner plasma flow is surrounded by a slower moving one (Sol et al. 1989; Laing 1996; Paraschos et al. 2024a). In this case, the

² https://fermi.gsfc.nasa.gov/ssc/data/access/lat/msl_1c/

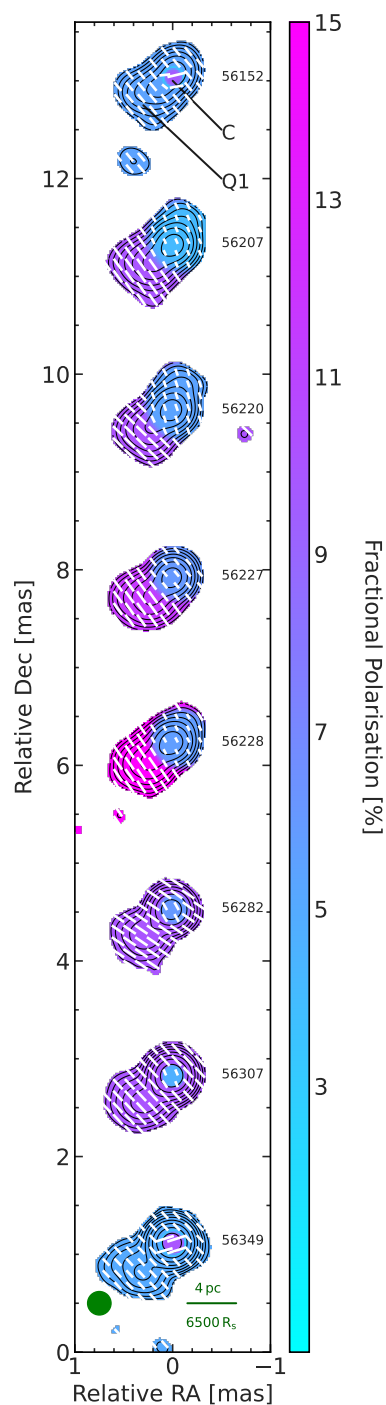


Fig. 1: Stokes I image (contours) and fractional polarisation geometrical model-fit (colour) of OJ 248 showcasing the epochs close in time to the MJD 56152–56349 (year: 2012–2013) γ -ray flare. The colour scale is linear and the units are in %. The dark green ellipse in the lower left corner shows the common convolving circular beam size of 0.24 mas. The green bar (bottom right) corresponds to a projected distance of $6500R_S$ (Schwarzschild radius). Superimposed are the EVPAs (white sticks), showcasing the direction of the electric field and by extension that of the magnetic field (perpendicular). Their length is proportional to the fractional polarisation values. The lowest Stokes I contour cutoff is at $5\sigma_1$ is implemented, to only include high S/N areas (with $\sigma_1 = 0.71$ mJy/beam). The contour levels are at 0.25, 0.5, 1, 2, 4, 8, 16, 32, and 64% of the total intensity peak per epoch, the MJDs of which are denoted next to each observation. The core C and component Q1 are denoted in the first epoch. The EVPAs in C start out along the bulk jet flow (southeast direction). As the shock front progresses downstream, they exhibit a clear turn, becoming perpendicular to the bulk jet flow and aligned to the EVPAs in Q1.

Table 1: Summary of the component parameters

ID	Obs. [MJD - 50000]	F0 [Jy]	FWHM [mas]	Position [mas, mas]	Frac. pol [%]	EVPA [deg]
C	6152	0.240 ± 0.036	0.03 ± 0.048	[0.00, 0.00]	9.9 ± 1.5	104 ± 6
C	6207	0.550 ± 0.083	0.10 ± 0.048	[0.00, 0.00]	4.1 ± 0.6	24 ± 6
C	6220	0.570 ± 0.085	0.09 ± 0.048	[0.00, 0.00]	5.3 ± 0.8	19 ± 6
C	6227	0.558 ± 0.084	0.08 ± 0.048	[0.00, 0.00]	6.0 ± 0.9	40 ± 6
C	6228	0.570 ± 0.085	0.08 ± 0.048	[0.00, 0.00]	5.7 ± 0.9	28 ± 6
C	6282	0.479 ± 0.072	0.04 ± 0.048	[0.00, 0.00]	6.0 ± 0.9	29 ± 6
C	6307	1.094 ± 0.164	0.02 ± 0.048	[0.00, 0.00]	4.7 ± 0.9	23 ± 6
C	6349	1.855 ± 0.278	0.03 ± 0.048	[0.00, 0.00]	10.0 ± 3.9	108 ± 6
Q1	6152	0.314 ± 0.047	0.20 ± 0.048	[0.15, -0.08]	5.4 ± 0.8	40 ± 6
Q1	6207	0.290 ± 0.043	0.21 ± 0.048	[0.21, -0.16]	10.0 ± 1.5	36 ± 6
Q1	6220	0.231 ± 0.035	0.19 ± 0.048	[0.22, -0.16]	10.1 ± 1.5	46 ± 6
Q1	6227	0.251 ± 0.038	0.19 ± 0.048	[0.21, -0.17]	11.6 ± 1.7	36 ± 6
Q1	6228	0.242 ± 0.036	0.19 ± 0.048	[0.22, -0.15]	15.0 ± 2.3	34 ± 6
Q1	6282	0.109 ± 0.016	0.19 ± 0.048	[0.20, -0.14]	10.0 ± 1.5	56 ± 6
Q1	6307	0.190 ± 0.029	0.19 ± 0.048	[0.22, -0.22]	10.0 ± 1.5	43 ± 6
Q1	6349	0.140 ± 0.021	0.22 ± 0.048	[0.23, -0.02]	5.0 ± 0.8	43 ± 6

blazar zone might be connected to either the spine or the sheath (see, e.g. [Blandford et al. 2019](#), for a review).

A common strategy of localising the blazar zone is to study the correlation between the onset and duration of a multi-band flare at the different frequency bands. Interestingly, as discussed in [Carnerero et al. \(2015\)](#), the OJ 248 multi-band light curves recorded in γ -rays, optical, IR, and radio bands have exhibited a significant correlation over time, when taking into account the source's past main flaring events. Such a manifestation is commonplace for blazars like OJ 248 ([León-Tavares et al. 2011](#)). The simultaneity of this multi-band flare and the activity in the jet dynamics found in our work strongly indicates a connection between them. A natural explanation of this phenomenon is that the blazar region is optically thin to radio wavelengths. The increase of the fractional polarisation in Q1 and the EVPAs' rotation in C can be explained by a moving shock front, as reported, for example, in [Liodakis et al. \(2022\)](#). This shock front then appears to be ripping through a standing recollimation shock in the vicinity of the VLBI core ([Daly & Marscher 1988](#)), resulting also in the observed peak multiplicity of the γ -rays (see middle and bottom panel of Fig. 2). Such activity has also been reported for the case of PKS 1510-089 in [H. E. S. S. Collaboration et al. \(2021\)](#). We note with interest, that a similar such morphology has also been reported in other sources (e.g. [Larionov et al. 2013](#); [Liodakis et al. 2020](#)).

At this point we can additionally consider two alternative scenarios for the observed behaviour, namely either a kink instability ([Nalewajko 2017](#)), or geometric effects. For the former we would expect a decrease in optical polarisation, which is not reported in [Carnerero et al. \(2015\)](#). A swinging nozzle model, in which abrupt changes to the viewing angle result in the flux density increase in all bands, has been proposed by [Jorstad & Marscher \(2004\)](#) to explain the latter scenario for OJ 248. The

expected accompanying intranight variability, however, has been lacking (as reported in [Marchesini et al. 2016](#)).

Another ansatz is the commonly invoked shock-in-jet model [Marscher & Gear \(1985\)](#), which offers a convincing explanation of the increase in optical polarisation, as well as in fractional polarisation in the time frame of the γ -ray flare. In that case, the travelling shock front is expected to compress the magnetic field component perpendicular to the outflow and to cause a rotation of the optical EVPAs ([Blinov et al. 2018](#)). However, similarly to the case of the radio sources 3C 454.3 ([Liodakis et al. 2020](#)) and S4 0954+65 ([Kouch et al. 2024](#)), in OJ 248 the EVPAs are the ones directed perpendicular to jet flow direction, which means that the magnetic field lines are parallel to it. Therefore, with the addition of the case of OJ 248 to the above two, there is now mounting evidence of the scenario described in [Marscher et al. \(2002\)](#). In that work, the authors postulate that ambient magnetic field lines parallel to the jet axis are possibly amplified by shearing processes or interactions with the surrounding medium. A passing shock front would then result in increased particle acceleration, which leads to the observed geometry of the EVPAs in C. We propose here that this description fits the observed phenomenology; the shock propagates through and beyond C, which harbours an area of magnetic field lines parallel to the bulk jet flow. Particles are accelerated and then cool down, causing the γ -ray flare in this region of magnetic field lines streamlined to the jet axis. Furthermore, in this interpretation the magnetic field is not amplified (no compression to amplify the magnetic flux takes place), explaining the lower fractional polarisation values of C during the γ -ray flare. Finally, at the decay phase of the γ -ray flare, the magnetic field that the shock interacts with becomes more turbulent. This results in the compression of the field, providing order and restoring the EVPA orientation parallel to the bulk jet flow (see [Kouch et al. 2024](#)), which explains the observed rise of fractional polarisation in C after the flare.

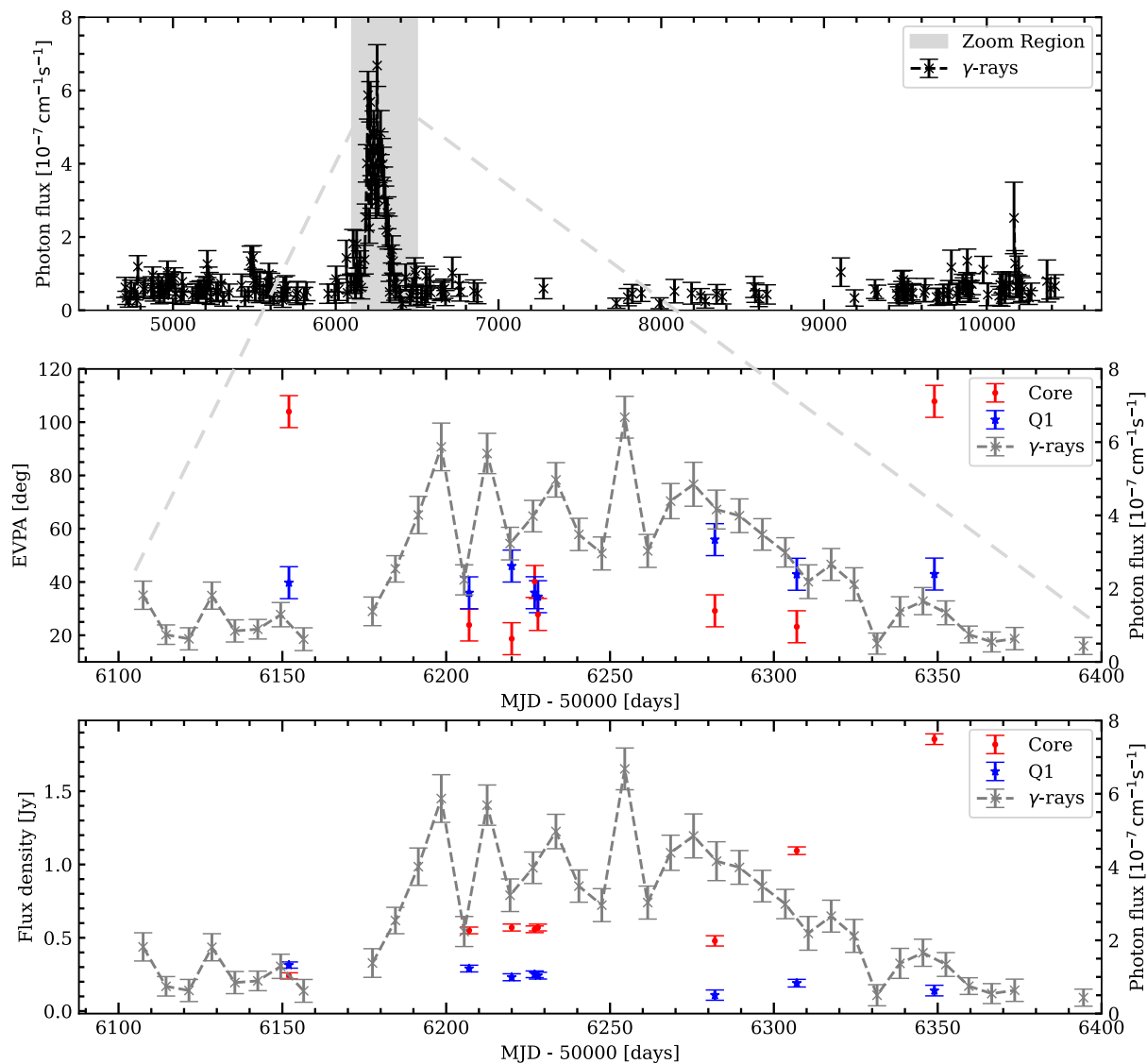


Fig. 2: OJ 248 component EVPAs and flux density, and the Fermi γ -ray-LAT light curve. *Top*: The grey-shaded area emphasises the period in question, when the prominent γ -ray flare occurred. In the years after, the source has remained quiescent. *Middle*: The zoom-in of the γ -ray flare time frame (grey-shaded area of the top panel), revealing a multiple peaked profile. Additionally, the EVPAs in C (red) and Q1 (blue) were perpendicular to each other immediately before and after the γ -ray flare, but then rotated to be aligned during the flaring event. *Bottom*: Same zoom-in region as above with the flux density of C denoted in red and the one for Q1 in blue. An increasing trend in C is identified.

Overall, the rotation of the EVPAs in the central region C being simultaneous with the increase in polarisation of the jet (Q1), is evidence in favour of the blazar region of OJ 248 being in the vicinity of the 43 GHz VLBI core. In our present understanding of blazar jets (e.g. Marscher et al. 2008) this corresponds to a \sim parsec-scale distance to central engine. Below, we also consider sub-parsec scale distances for the blazar zone. Specifically, the dusty torus, a possible source of seed electrons needed to cause the γ -ray flare (Saito et al. 2015; Ahnen et al. 2017), would be located too far upstream, close to the central engine. Similarly, a blazar region supported by photons from the broad line region, as suggested by Ghisellini & Madau (1996), would require the γ -ray flare to lag the optical one, which is not conclusively observed in Carnerero et al. (2015). Finally, if the blazar

zone is located even further downstream (few parsec away from the central engine), as indicated by the evolution of the jet seen in Fig. 1, the origin of the seed photons could be within a surrounding jet sheath (e.g. Attridge et al. 1999; MacDonald et al. 2015). This scenario, which particularly works for FSRQs such as OJ 248, has been reported to be able to produce the observed γ -ray flares (MacDonald et al. 2017), albeit in a suppressed magnetic field strength regime. In that case, we can also make a prediction about future γ -ray flares in the source, based on the work presented by Blinov et al. (2021). Specifically, the authors there show that condensation rings within the jet sheath, surrounding the inner spine, can provide the necessary seed photons. Under these model assumptions, future γ -ray flares are predicted to exhibit a similar pattern to the one found here (i.e. multiple peaks).

4. Conclusions

In this work we investigated the connection between the polarisation properties of the OJ 248 jet and a prominent γ -ray flare detected in the same source. Our findings can be summarised as follows:

- The OJ 248 jet exhibits remarkable morphological changes through the course of the flaring event, detected in γ -rays, optical, near infrared, and radio bands, as well as in polarised emission. Specifically, the VLBI fractional linear polarisation of its extended emission (component Q1) is heightened during the γ -ray outburst, while being in lower states immediately before and after. The EVPAs appear to also be affected; during the γ -ray flare they are perpendicular to the bulk jet flow, whereas before and after they are not.
- This behaviour is consistent with a moving shock front, travelling through a recollimation shock, while causing the photons to be inverse Compton upscattered into creating the γ -ray flare.

Our work presented here showcases the importance of monitoring blazars both with VLBI and with individual telescopes at multiple bands, in order to gain insights into their underlying physical mechanisms. Future, higher sensitivity instruments, such as the next-generation Very Large Array (ngVLA) will enable us to image fainter sources, such as OJ 248, in greater detail and thus leverage the possibilities that multi-messenger astronomy has ushered in.

Acknowledgements. We thank I. Liodakis and an anonymous referee for their valuable comments which greatly improved this manuscript and L. Debbrecht for the insightful discussions. This research is supported by the European Research Council advanced grant “M2FINDERS - Mapping Magnetic Fields with Interferometry Down to Event Horizon Scales” (Grant No. 101018682). This study makes use of VLBA data from the VLBA-BU Blazar Monitoring Program (BEAM-ME and VLBA-BU-BLAZAR; <http://www.bu.edu/blazars/BEAM-ME.html>), funded by NASA through the Fermi Guest Investigator Program. The VLBA is an instrument of the National Radio Astronomy Observatory. The National Radio Astronomy Observatory is a facility of the National Science Foundation operated by Associated Universities, Inc. This research has made use of the NASA/IPAC Extragalactic Database (NED), which is operated by the Jet Propulsion Laboratory, California Institute of Technology, under contract with the National Aeronautics and Space Administration. This research has also made use of NASA’s Astrophysics Data System Bibliographic Services. Finally, this research made use of the following python packages: *numpy* (Harris et al. 2020), *scipy* (Virtanen et al. 2020), *matplotlib* (Hunter 2007), *astropy* (Astropy Collaboration et al. 2013, 2018) and *Uncertainties: a Python package for calculations with uncertainties*.

References

Abdo, A. A., Ackermann, M., Ajello, M., et al. 2010, *ApJ*, 716, 835
 Agudo, I. 2013, in *European Physical Journal Web of Conferences*, Vol. 61, European Physical Journal Web of Conferences, 04002
 Ahnen, M. L., Ansoldi, S., Antonelli, L. A., et al. 2017, *A&A*, 603, A25
 Ajello, M., Angioni, R., Axelsson, M., et al. 2020, *ApJ*, 892, 105
 Astropy Collaboration, Price-Whelan, A. M., Sipőcz, B. M., et al. 2018, *AJ*, 156, 123
 Astropy Collaboration, Robitaille, T. P., Tollerud, E. J., et al. 2013, *A&A*, 558, A33
 Attridge, J. M., Roberts, D. H., & Wardle, J. F. C. 1999, *ApJ*, 518, L87
 Atwood, W. B., Abdo, A. A., Ackermann, M., et al. 2009, *ApJ*, 697, 1071
 Blandford, R., Meier, D., & Readhead, A. 2019, *ARA&A*, 57, 467
 Blinov, D., Jorstad, S. G., Larionov, V. M., et al. 2021, *MNRAS*, 505, 4616
 Blinov, D., Pavlidou, V., Papadakis, I., et al. 2018, *MNRAS*, 474, 1296
 Carnerero, M. I., Raiteri, C. M., Villata, M., et al. 2015, *MNRAS*, 450, 2677
 Chael, A. A., Johnson, M. D., Narayan, R., et al. 2016, *ApJ*, 829, 11
 Daly, R. A. & Marscher, A. P. 1988, *ApJ*, 334, 539
 Enya, K., Yoshii, Y., Kobayashi, Y., et al. 2002, *ApJS*, 141, 31
 Ghisellini, G. & Madau, P. 1996, *MNRAS*, 280, 67
 H. E. S. S. Collaboration, Abdalla, H., Adam, R., et al. 2021, *A&A*, 648, A23

Harris, C. R., Millman, K. J., van der Walt, S. J., et al. 2020, *Nature*, 585, 357
 Hewett, P. C. & Wild, V. 2010, *MNRAS*, 405, 2302
 Hovatta, T. & Lindfors, E. 2019, *New A Rev.*, 87, 101541
 Hunter, J. D. 2007, *Computing in Science & Engineering*, 9, 90
 Jorstad, S. G. & Marscher, A. P. 2004, *ApJ*, 614, 615
 Jorstad, S. G. & Marscher, A. P. 2006, *Astronomische Nachrichten*, 327, 227
 Jorstad, S. G., Marscher, A. P., Mattox, J. R., et al. 2001, *ApJ*, 556, 738
 Jorstad, S. G., Marscher, A. P., Morozova, D. A., et al. 2017, *ApJ*, 846, 98
 Königl, A. 1981, *ApJ*, 243, 700
 Kouch, P. M., Liodakis, I., Fenu, F., et al. 2024, *arXiv e-prints*, arXiv:2411.16868
 Läing, R. A. 1996, in *Astronomical Society of the Pacific Conference Series*, Vol. 100, *Energy Transport in Radio Galaxies and Quasars*, ed. P. E. Hardee, A. H. Bridle, & J. A. Zensus, 241
 Larionov, V. M., Jorstad, S. G., Marscher, A. P., et al. 2013, *ApJ*, 768, 40
 León-Tavares, J., Valtaoja, E., Tornikoski, M., Lähteenmäki, A., & Niépola, E. 2011, *A&A*, 532, A146
 Liodakis, I., Blinov, D., Jorstad, S. G., et al. 2020, *ApJ*, 902, 61
 Liodakis, I., Marscher, A. P., Agudo, I., et al. 2022, *Nature*, 611, 677
 MacDonald, N. R., Jorstad, S. G., & Marscher, A. P. 2017, *ApJ*, 850, 87
 MacDonald, N. R., Marscher, A. P., Jorstad, S. G., & Joshi, M. 2015, *ApJ*, 804, 111
 Marchesini, E. J., Andruchow, I., Cellone, S. A., et al. 2016, *A&A*, 591, A21
 Marscher, A. P. & Broderick, J. J. 1983, *AJ*, 88, 759
 Marscher, A. P. & Gear, W. K. 1985, *ApJ*, 298, 114
 Marscher, A. P., Jorstad, S. G., D’Arcangelo, F. D., et al. 2008, *Nature*, 452, 966
 Marscher, A. P., Jorstad, S. G., Mattox, J. R., & Wehrle, A. E. 2002, *ApJ*, 577, 85
 McCall, C., Jermak, H. E., Steele, I. A., et al. 2024, *MNRAS*, 528, 4702
 Nalewajko, K. 2017, *Galaxies*, 5, 64
 Paraschos, G. F., Debbrecht, L. C., Kramer, J. A., et al. 2024a, *A&A*, 686, L5
 Paraschos, G. F., Kim, J. Y., Wielgus, M., et al. 2024b, *A&A*, 682, L3
 Paraschos, G. F., Krichbaum, T. P., Kim, J. Y., et al. 2022, *A&A*, 665, A1
 Paraschos, G. F., Mpisketzis, V., Kim, J. Y., et al. 2023, *A&A*, 669, A32
 Paraschos, G. F., Wielgus, M., Benke, P., et al. 2024c, *A&A*, 687, L6
 Piner, B. G., Bhattarai, D., Edwards, P. G., & Jones, D. L. 2006, *ApJ*, 640, 196
 Price, R., Gower, A. C., Hutchings, J. B., et al. 1993, *ApJS*, 86, 365
 Raiteri, C. M., Ghisellini, G., Villata, M., et al. 1998, *A&AS*, 127, 445
 Rani, B., Jorstad, S. G., Marscher, A. P., et al. 2018, *ApJ*, 858, 80
 Roelofs, F., Johnson, M. D., Chael, A., et al. 2023, *ApJ*, 957, L21
 Saito, S., Stawarz, L., Tanaka, Y. T., et al. 2015, *ApJ*, 809, 171
 Sol, H., Pelletier, G., & Asseo, E. 1989, *MNRAS*, 237, 411
 Villata, M., Raiteri, C. M., Ghisellini, G., et al. 1997, *A&AS*, 121, 119
 Virtanen, P., Gommers, R., Oliphant, T. E., et al. 2020, *Nature Methods*, 17, 261
 Zhang, X., Xiong, D.-r., Gao, Q.-g., et al. 2024, *MNRAS*, 529, 3699